Nano Energy (2014) 6, 1–9

Available online at www.sciencedirect.com

ScienceDirect

journal homepage: www.elsevier.com/locate/nanoenergy

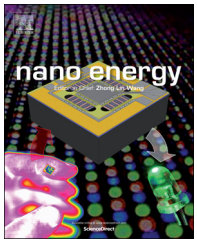

RAPID COMMUNICATION

# Freestanding functionalized carbon nanotube-based electrode for solid-state asymmetric supercapacitors

Xu Xiao[a,b], Tianqi Li[a], Zehua Peng[a], Huanyu Jin[a], Qize Zhong[a], Qiyi Hu[a], Bin Yao[a], Qiuping Luo[a], Chuanfang Zhang[b], Li Gong[c], Jian Chen[c], Yury Gogotsi[b], Jun Zhou[a,*]

[a]*Wuhan National Laboratory for Optoelectronics, School of Optical and Electronic Information, Huazhong University of Science and Technology, Wuhan 430074, PR China*
[b]*Department of Materials Science and Engineering, A.J. Drexel Nanomaterials Institute, Drexel University, Philadelphia, PA 19104, USA*
[c]*Instrumental Analysis & Research Center, Sun Yat-sen University, Guangzhou 510275, PR China*

Received 9 January 2014; received in revised form 25 February 2014; accepted 27 February 2014
Available online 12 March 2014

**KEYWORDS**
Functionalization;
Carbon nanotube;
Freestanding;
Asymmetric supercapacitor

**Abstract**
Recently, many attempts have been made to increase the specific capacitance of carbon nanotubes (CNTs). Chemical enhancement by adding redox active functional groups on CNTs increases the specific capacitance, while excessive oxidation decreases conductivity and leads to poor cycle life. Here we report the electrochemical enhancement methods followed by annealing at different temperatures in air to add and adjust the redox active functional groups on freestanding CNT films. Functionalized freestanding CNT films were used as positive electrodes, assembled with freestanding CNT/$MoO_{3-x}$ negative electrodes to fabricate carbon nanotube-based solid-state asymmetric supercapacitors (ASCs). The whole device showed a high volumetric capacitance of 3.0 F $cm^{-3}$, energy and power density of 1.5 mWh $cm^{-3}$ and 4.2 W $cm^{-3}$, respectively. We also fabricated a SCs pack to drive a homemade wireless transport system successfully, demonstrating the potential applications of this solid-state system for portable/wearable electronics.


*Corresponding author.
*E-mail address:* jun.zhou@mail.hust.edu.cn (J. Zhou).

http://dx.doi.org/10.1016/j.nanoen.2014.02.014
2211-2855/

## Introduction

Nowadays, the proliferation of portable/wearable electronics such as wearable displays and flexible sensor networks leads to increasing energy consumption and requires sustainable and portable energy storage devices [1-4]. Green energy from intermittent sources such as solar and wind also requires energy storage systems [5,6]. Supercapacitors (SCs) and batteries are the most common energy storage devices which have been researched for decades [7-11]. Benefiting from the high power density, fast charge/discharge rates and long cycle life, SCs would be favored in various applications, including but not limited to backup power, hybrid vehicles and pace makers [12]. Replacement of liquid electrolyte with solid-state electrolyte offers a promising way to fabricate flexible, lightweight and safe solid-state SCs, which are desirable for portable/wearable electronics [13-17].

By virtue of high conductivity, high specific area, low specific weight and mechanical integrity, carbon nanotubes (CNTs) have attracted the scientific and commercial interest worldwide in fields such as flexible electronics and energy storage [18,19]. However, the low specific capacitance of CNTs hinders their applications as electrodes for high energy SCs [20]. Although chemical enhancement by adding redox active functional groups on CNTs increases the specific capacitance, excessive oxidation decreases conductivity and leads to poor cycle life [21-24]. In this context, it is necessary to develop a stable CNT electrode with high specific capacitance without sacrificing the high power density and long term stability.

Herein, we adopted the electrochemical enhancement methods followed by annealing at different temperatures in air to add and adjust the redox active functional groups on freestanding CNT films. A systematic study of the influence of different functional groups content on electrochemical performance, conductivity and cycle life was also performed. Furthermore, we used functionalized freestanding CNT films as the positive electrodes, assembled with freestanding CNT/$MoO_{3-x}$ negative electrodes to fabricate high performance carbon nanotube-based solid-state asymmetric SCs (ASCs). The whole device, including the electrodes, electrolyte and separator, showed a high volumetric capacitance of 3.0 F $cm^{-3}$, high energy and power density of 1.5 mWh $cm^{-3}$ and 4.2 W $cm^{-3}$, respectively, with a stable operation window between 0 and 1.9 V. We also fabricated a SCs pack to drive a homemade wireless transport system successfully, demonstrating the potential applications of this solid-state system for portable/wearable electronics.

## Experimental

### Preparation of functionalized freestanding CNT films

We used the vacuum filtration method to fabricate the flexible freestanding CNTs films. 0.1 g SDBS used as surfactant was dissolved in DI water (50 mL) containing CNTs (0.050 g, Blue Nano, China), then probe sonicated for 20 min to form CNT ink. The as-obtained solution was filtered through a membrane (220 nm pore size). The obtained filter cake was dried in vacuum for 0.5 h and then peeled off to obtain a freestanding film. After that, the samples were cut into pieces of 1.4 cm × 0.7 cm and treated by an efficient electrochemical enhancement method. A typical three-electrode configuration with freestanding CNT films as the working electrode, Ag/AgCl electrode as the reference electrode, a graphite rod as the counter electrode and 1 M $H_2SO_4$ aqueous solution as the electrolyte was tested at 2.2 V for 20 min. After that we got the functionalized freestanding CNT films.

### Assembly of the solid-state symmetric and asymmetric SCs

A functionalized freestanding positive electrode was assembled with CNT/$MoO_{3-x}$ as negative electrode to fabricate a solid-state ASC. PVA/LiCl gel was prepared by mixing LiCl (12 g) and

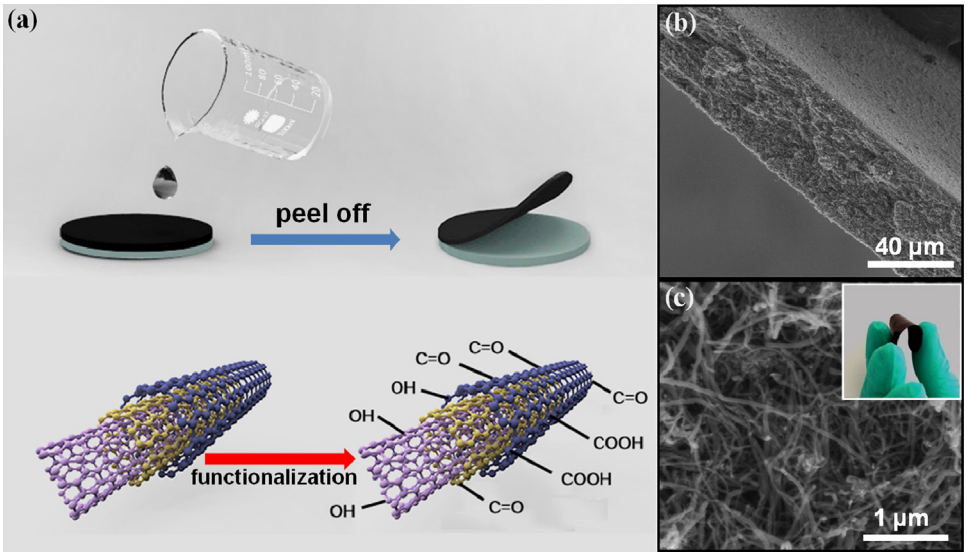


**Figure 1** (a) Schematic of the fabrication procedure for functionalized freestanding CNT films. (b) Cross-section SEM image of the functionalized freestanding CNT film. (c) Enlarged cross-section SEM image of the functionalized freestanding CNT films. The inset is digital image of a functionalized freestanding CNT film.

PVA (6 g) in deionized water (60 mL) and heated at 85 °C under vigorous stirring until the solution became clear. Two electrodes were immersed in PVA/LiCl gel for 5 min then assembled together and separated by a cellulose separator (NKK TF40, 40 μm). The symmetric SCs for cycle life measurements in Figure 3d were fabricated by using two functionalized CNT electrodes, following the same process as above.

## Characterizations

The morphology and structure of the samples were studied by field-emission scanning electron microscopy (FE-SEM, FEI Nova 450 Nano) and high-resolution transmission electron microscopy (HRTEM, TECNAI). The content of the functional groups was determined by thermogravimetric analysis (TGA, Pyris1), Fourier transform infrared absorption spectroscopy (FTIR, VERTEX 70) and X-ray photoelectron spectroscopy (XPS, ESCALab250). There are no functional groups on sample P found by FTIR, while there were functional groups observed in the XPS measurement. The sample P analyzed by FTIR was fabricated by mixing pure CNTs (no functional groups) with KBr. However, we used the freestanding film for XPS measurement, and the functional groups on sample P (XPS) could come from the physisorption of water during the sample preparation (O/C ratio was only 0.05). The relative content of functional groups was calculated by dividing the area integral of the functional group peak over the area of the O1s peak. The O/C ratio was calculated by the area of the O1s peak divided by the area of the C1s peak. All of the electrochemical tests were carried out using Autolab PGSTAT302N. Electrochemical impedance was measured from 1 mHz to 1 MHz with a potential amplitude of 10 mV.

## Results and discussion

The fabrication process of the functionalized freestanding CNT films is illustrated in Figure 1a. Firstly, desired amounts of CNTs and sodium dodecylbenzenesulfonate (SDBS) were dispersed in deionized water following with probe sonication to form CNT ink. The ink solution was then vacuum-filtered through a membrane. After vacuum drying, paper-like freestanding CNT films were obtained by peeling off from the filter membrane [25,26]. We adopted the efficient electrochemical enhancement methods to add redox active functional groups on CNT films. Briefly, a typical three-electrode configuration with freestanding CNT films as the working electrode, Ag/AgCl electrode as the reference electrode, a graphite rod as the counter electrode and 1 M $H_2SO_4$ aqueous solution as the electrolyte was oxidized at 2.2 V for 20 min regardless of water splitting. After washed in deionized water, the functionalized freestanding CNT films were annealed in air at different temperatures to adjust the types and amount of functional groups. The scanning electron microscopy (SEM) images of the as-fabricated functionalized freestanding CNT films are shown in Figure 1b and c. According to Figure 1b, the cross-section SEM image revealed a uniform film with a thickness of 45 μm. Figure 1c is the enlarged cross-section SEM image, indicating that the CNTs were well linked together and distributed uniformly. Used as both, the active material and current collector, the interpenetrating structure has hierarchical porous channels, enabling electrolyte absorption and active-site accessibility, facilitating effective electron transport. The inset shows the digital images of the functionalized freestanding CNT film, which could perform highly flexibility without any obvious mechanical damage after bending.

Firstly, TGA was conducted as shown in Figure S1a. Owing to the detachment of functional groups, the weight loss appeared around 100, 200, 300 and 400 °C. The types and amount of functional groups on CNT films were characterized by FTIR and XPS, as shown in Figures S1b, S2 and 2a. The pure CNT film, functionalized CNT film without annealing, functionalized CNT film with annealing at 100, 200, 300 and 400 °C were denoted as sample P, UA, 100, 200, 300 and 400, respectively. According to FTIR spectra, carbonyl (>C═O), hydroxyl (>COH), and carboxy (-COOH) group were found in all samples except sample P. In addition, XPS confirmed the existence of these functional groups which were positioned at 531.6 eV (>C═O), 532.9 eV (>COH) and 534.2 eV (-COOH), respectively [27]. To evaluate the impact of annealing on the functional groups, we calculated the O/C ratio and functional groups distribution from the XPS data. According to Figure 2b, O/C ratio decreased monotonically with the increasing temperature, demonstrating the removal of oxygen-containing functional groups during

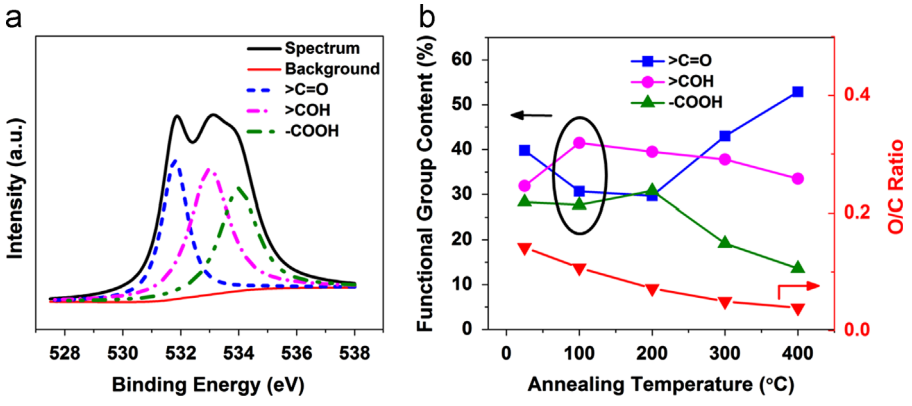


**Figure 2** (a) XPS spectrum of sample 200. (b) O/C ratio and functional groups content for sample UA, 100, 200, 300 and 400. The functionalized CNT film without annealing, functionalized CNT film with annealing at 100, 200, 300 and 400 °C were denoted as sample UA, 100, 200, 300 and 400, respectively.

annealing. The relative content of >COH and -COOH increased first and then decreased while >C=O had the opposite trend. As the temperature increased, the bond of functional groups ruptured based on their thermal stability. From room temperature (sample UA) to 100 °C, the major process was the desorption of physisorbed water. -COOH and >C=O can only exist at the edges or defects of CNTs, while >COH can exist on the basal plane and the edge plane [28]. Specially, the >COH on the basal plane causes the rehybridization from $sp^2$ to $sp^3$ state which strain loads and the >COH on the basal plane becomes unstable. When the annealing temperature increased to 200 °C, owing to conjugate π bond, -COOH and >C=O on the edge plane were more stable than the >COH on the basal plane, the >COH would largely desorbs from the basal plane, sending the electron from σ bond to delocalized π bond, which could increase the conductivity of CNTs. On the other hand, bonding energy of >C=O is lower than that of -COOH, leading to easier detachment of >C=O compared to -COOH. Accordingly, the relative content of -COOH was the highest at 200 °C. From 200 °C to 400 °C, -COOH would transform to >C=O due to acid dehydration, resulting in the increasing relative content of >C=O.

In order to probe the electrochemical performance of different samples, cyclic voltammetry (CV), galvanostatic charge-discharge (GCD) electrochemical impedance spectroscopy (EIS) and cycle life measurements were conducted. All the samples were cut into the same size (1.4 cm × 0.7 cm) and tested in a three-electrode configuration with samples as the working electrodes, Ag/AgCl electrode as the reference electrode, a graphite rod as the counter electrode and 0.5 M $Na_2SO_4$ aqueous solution as the electrolyte. CV curves of sample 200 with scan rates from 10 mV $s^{-1}$ to 100 mV $s^{-1}$ under a stable operation window between 0 and 0.9 V are shown in Figure 3a, exhibiting a roughly rectangular shape approximately symmetrical about the zero-current line, indicating the good electrochemical behavior. Figure 3b reveals the GCD curves, through which the areal capacitance of the SCs could be calculated by the following equations (Figures 3b and S3):

$$C = I\Delta t/\Delta U \quad (1)$$

$$Cs = C/S = I\Delta t/S\Delta U \quad (2)$$

where $C$ is the total capacitance, $I$ is the discharge current, $\Delta t$ is the discharge time, $\Delta U$ is the potential window during the discharge process after $IR$ drop, and $S$ is the working area of the sample. It should be easily understood that the conductivity of sample UA was so poor with so many functional groups, resulting in no capacitance. The areal capacitance of sample 200, compared with others, was the highest (Figure 3c). Generally, the oxygen-containing functional groups could improve the specific capacitance by adding reversible faradic reactions (pseudocapacitance). However, as positive electrodes, oxidation reaction should occur during charging. Frackowiak and Béguin pointed the faradic reactions of >COH, -COOH and >C=O, through

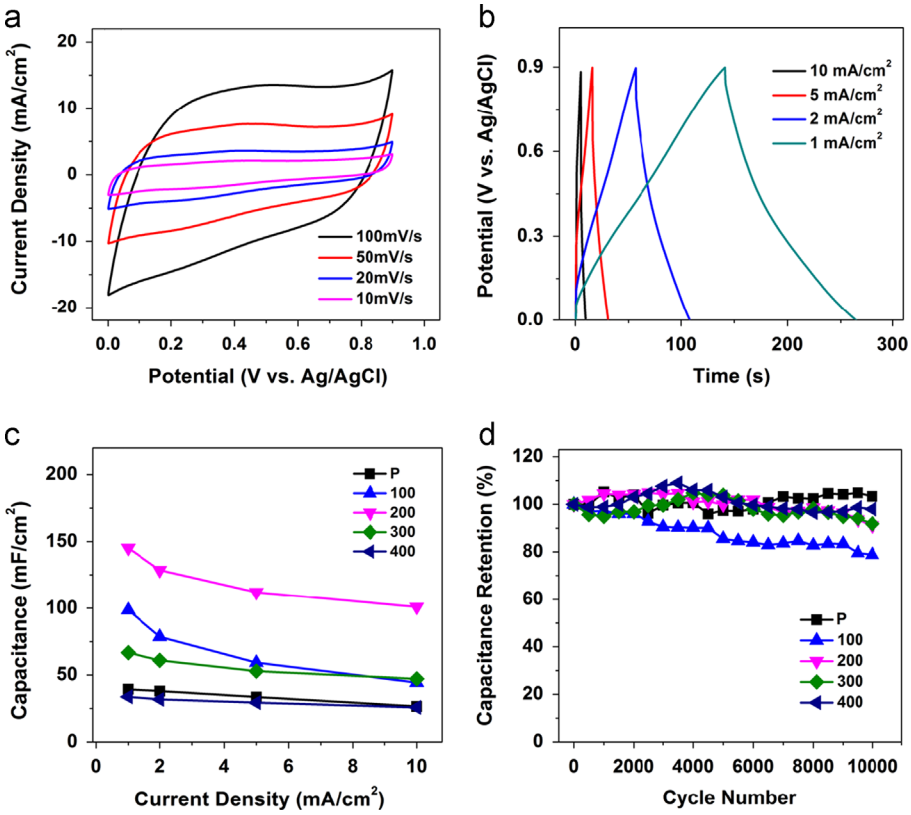


**Figure 3** The electrochemical performance which was tested in single electrode-configuration in liquid electrolyte. (a and b) CV and GCD curves for sample 200. (c) Capacitance with respect to current density for different samples. (d) Cycle life measurements for different samples which were tested in symmetric solid-state SCs. The pure CNT film, functionalized CNT film with annealing at 100, 200, 300 and 400 °C were denoted as sample P, 100, 200, 300 and 400, respectively.

which >COH and -COOH could provide reversible pseudocapacitance as positive electrode by the following reactions while >C=O could not [20].

$$>COH \Leftrightarrow >C=O+H^{+}+e^{-} \quad (3)$$

$$-COOH \Leftrightarrow -COO+H^{+}+e^{-} \quad (4)$$

Accordingly, the content of >COH and -COOH in samples 100 and 200 was much higher than others, resulting in the higher areal capacitance (capacitance of sample 100 under low current density). However, from 100 °C to 200 °C, the charge transfer resistance (CTR) decreased from 8.6 Ω to 2.1 Ω (Figure S4) due to transformation from σ bond to delocalized π bond. The relatively poor conductivity hindered the electron and charge transport in sample 100, leading to a lower capacitance than sample 200 and poor rate capability. The capacitance decreased with decreasing content of functional groups in sample 300 and 400, and a relatively higher CTR in sample 400 (possibly due to the defects from electrochemical oxidation) leads to somewhat lower capacitance than sample P. We also measured the cycle life of different samples for 10,000 charge/discharge cycles. All of the samples were fabricated into solid-state devices to demonstrate their long-term stability in solid-state electrolyte for the following experiments' consideration. According to Figure 3d, device UA and 100 revealed a relatively poor stability which may be attributed to a poor conductivity caused by large member of >COH groups on the basal plane. The poor conductivity would form uneven distribution of voltage, leading to hyperpolarization. Some functional groups would decompose due to hyperpolarization, which leads to poor stability. To sum up, the sample 200 showed the highest volumetric capacitance with excellent conductivity and long-term stability, becoming a good candidate as a positive electrode for ASCs.

Contemporarily, the limited working voltage window and energy density of SCs would inhibit the attempt to utilize the SCs as high performance power sources in practical applications [29]. Since the energy density can be calculated as

$$E = 0.5C(\Delta U)^2 \quad (5)$$

enhancement of energy density can be achieved by fabricating ASCs, expanding the working voltage window and increasing energy density by combining two appropriate electrodes with different operation windows [30]. In previous work, $MoO_{3-x}$ was demonstrated as a good negative electrode material with a large operation window and a high specific capacitance, therefore, we used electrodeposition to form a freestanding CNT/$MoO_{3-x}$ hybrid structure negative electrode (Figure S5a) [8,29,31]. According to the energy dispersive X-ray spectroscopy (EDAX) mapping in Figure S5b-d, the C, Mo and O signals were found, demonstrating the homogeneous formation of CNT/$MoO_{3-x}$ hybrid structure. Figure S5e shows the XPS spectrum of Mo 3d, in which two strong peaks corresponded to $Mo^{6+}$ and a weak peak corresponded to $Mo^{5+}$. The CVs of the freestanding CNT/$MoO_{3-x}$ electrode was recorded in a three-electrode configuration with an Ag/AgCl reference electrode, a graphite rod as the counter electrode and 0.5 M aqueous $Na_2SO_4$ electrolyte (Figure S5f).

The electrochemical performance of the solid-state ASCs was carefully evaluated through CV, GCD and cycle life measurements. The volume and weight of the whole device (including the electrodes, electrolyte and separator) were about 0.015 $cm^3$ (1.4 cm × 0.7 cm × 0.015 cm) and 20 mg,

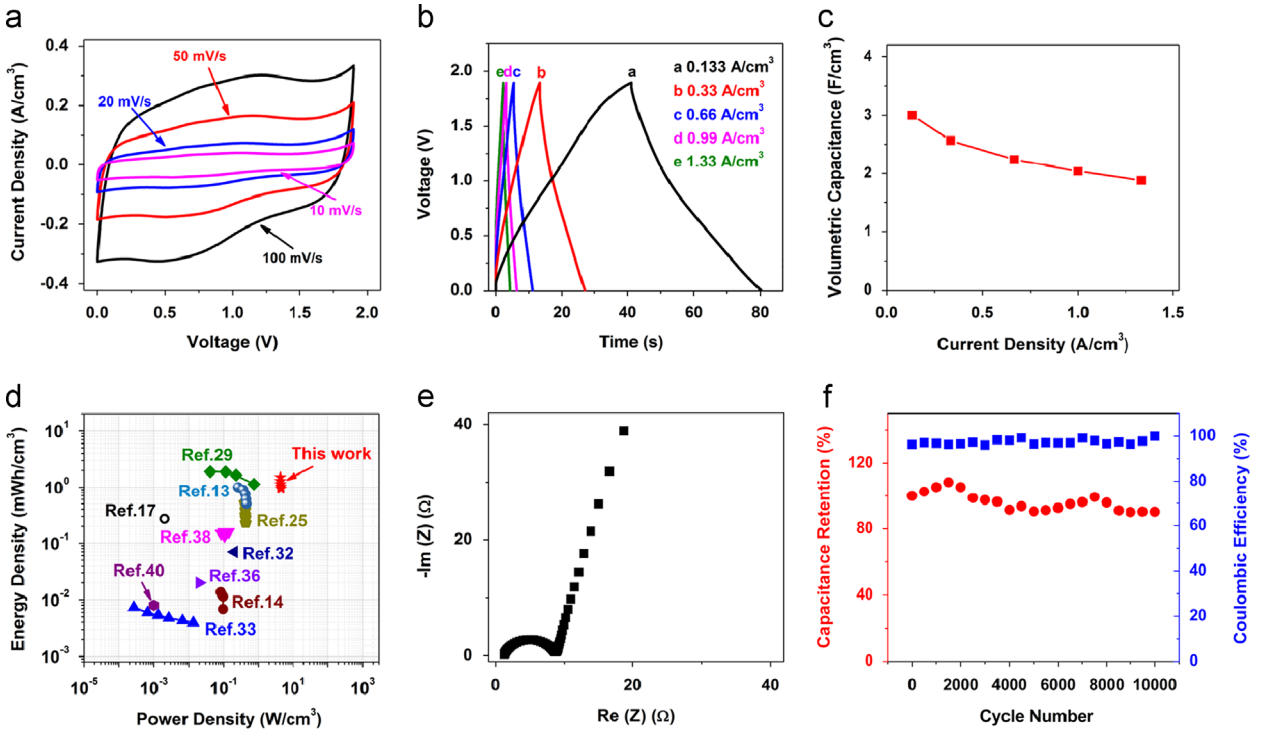


**Figure 4** The electrochemical performance of the ASC device. (a) CV scans at rates from 10 to 100 mV/s. (b) Galvanostatic charge/discharge curves. (c) Volumetric capacitance versus current density. (d) Ragone plot of the ASC device compared with other solid-state devices. (e) Nyquist plot and (f) cycle life.

respectively. The CV curves of the solid-state ASCs with scan rates from 10 to 100 mV $s^{-1}$ at stable working voltage window 0-1.9 V is shown in Figure 4a. GCD curves under different current density are shown in Figure 4b, through which the volumetric capacitance could be obtained. The solid-state ASCs revealed the highest volumetric capacitance of 3.0 F $cm^{-3}$ at 0.133 A $cm^{-3}$ and remained at 1.9 F $cm^{-3}$ at 1.33 A $cm^{-3}$ discharge current density, which was much higher than the value reported for other solid-state symmetric SCs or ASCs [29,32-36]. The Ragone plot shown in Figure 4d shows the volumetric energy density versus the power density, which can be calculated by the following equations:

$$E = 0.5C(\Delta U)^2/V \quad (6)$$

$$P = 0.25(\Delta U)^2/VR \quad (7)$$

$$R = \Delta U_{drop}/2I \quad (8)$$

where $C$ is the total capacitance of the cell, which can be achieved through Eq. (1), $\Delta U$ is the cell voltage, $V$ is the volume of the whole device, and $R$ is the internal resistance of the devices estimated from the voltage drop ($\Delta U_{drop}$) at the beginning of the discharge at a constant current density ($I$). The highest volumetric energy density achieved was 1.5 mWh $cm^{-3}$ which is substantially higher than graphene [17,32], carbon nanotubes [36,37], $WO_{3-x}$/Au/$MnO_2$ core shell nanowires [14] VN [25], $MnO_2$/carbon fiber [33] and conductive polymer [13,38] based solid-state symmetric SCs and comparable with $WO_{3-x}$/$MoO_{3-x}$ based solid-state ASCs [29]. The highest volumetric power density was about 4.2 W $cm^{-3}$ which was much higher than other solid-state SCs and ASCs, as shown in Ragone plot. Both the high volumetric energy and power density indicated the potential applications for driving portable/wearable electronics. The charge transfer resistance was about 8 Ω obtained from nyquist plot (Figure 4e). In addition, the ASC device showed lifetime maintaining at 90% of initial capacity after 10,000 charge/discharge cycles at 0.5 A $cm^{-3}$ and the Coulombic efficiency remained close to 100% (Figure 4f).

Recently, many groups reported the use of SCs to power low energy electronics such as light-emitting-diodes (LED), small sensors and simple sensor systems [33,38], while it would be more significant to power some energy-thirsty electronics [39,40]. To prove the feasibility, we built a wireless transport system as shown in Figure 5a. Briefly, a sound signal was processed by frequency modulation system and emitted through an antenna. In our experiment, the emitted signal from a cell phone was tuned to 105 MHz and we used a radio to receive the signal. Figure 5b shows images of the wireless transport system, which needed rated voltage and current of 3.5 V and 3 mA, respectively. We fabricated a pack of 9 ASCs in series and parallel to meet the rated power of the wireless transport system. The voltage-time curve of the sound signal input is shown in Figure 5c, three single tones were introduced with different intervals. According to Figure 5d, which shows voltage-time curve of the received signal from the radio, the shape of three tones was almost unchanged and the intervals were identical compared to Figure 5c, demonstrating the successful sound signal transport from the cell phone to the radio. Actually, after charging for 1 min, the pack could power the wireless transport system for more than 30 s.

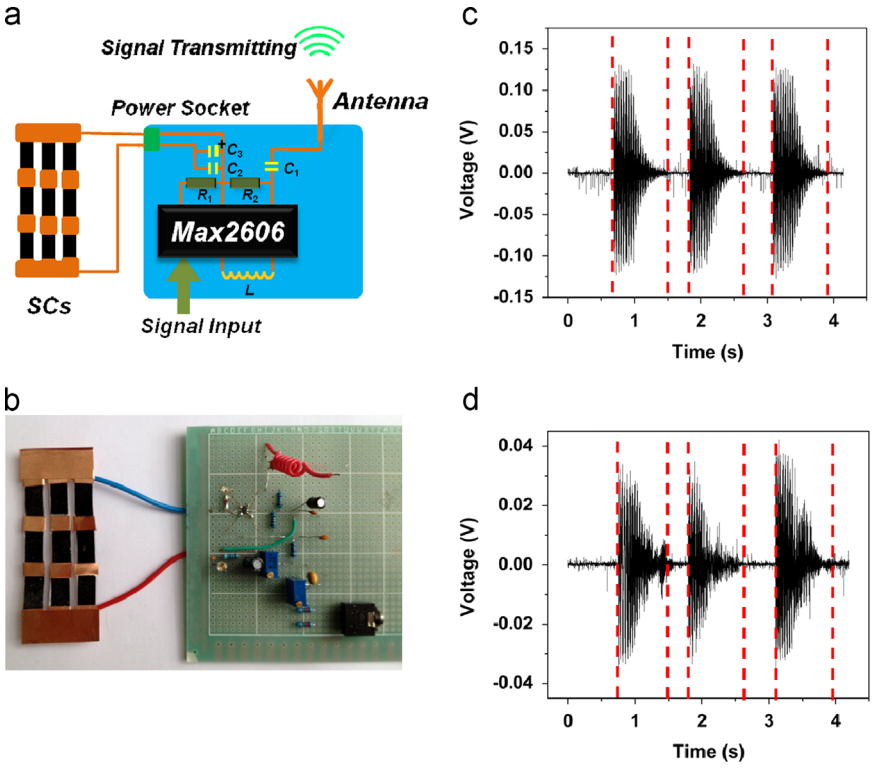


**Figure 5** (a) Structure chart of the wireless transport system. (b) Digital image of the wireless transport system. (c and d) The voltage-time curves for the input signal and received signal, respectively. C: commercial capacitor, R: resistance, L: inductance, Max2606: voltage-controlled oscillator.

## Conclusions

In conclusion, the electrochemical enhancement followed by annealing at different temperatures in air was used to add and adjust the number of >C=O, >COH and -COOH groups on freestanding CNT films. The highest electrochemical performance and stable long-term stability was achieved after annealing at 200 °C, which could be attributed to the relatively high content of >COH and -COOH groups adding pseudocapacitance and increasing high conductivity compared to other samples. Furthermore, carbon-based solid-state ASCs were fabricated by assembling functionalized freestanding CNT films as the positive electrodes with freestanding CNT/$MoO_{3-x}$ hybrid structure electrodes. The whole device showed high electrochemical performance, including a high volumetric capacitance of 3.0 F $cm^{-3}$, high energy and power density of 1.5 mWh $cm^{-3}$ and 4.2 W $cm^{-3}$, respectively, with a stable operation window between 0 and 1.9 V and long-term stability. We also applied a SCs pack to drive a home-made wireless transport system, indicating the potential applications as energy storage system for portable/wearable electronics.

## Acknowledgments

This work was financially supported by the National Natural Science Foundation of China (51322210, 51002056), a Foundation for the Author of National Excellent Doctoral Dissertation of PR China (201035), and the Fundamental Research Funds for the Central Universities (HUST: 2012YQ025, 2013YQ049, 2013TS160). The authors would also thank Miss Wenyuan Zhong and Prof. K.F. Huo from Huazhong University of Science and Technology for their help. The authors thank to the facility support of the Center for Nanoscale Characterization & Devices (CNCD), WNLO-HUST and the Analysis and Testing Center of Huazhong University of Science and Technology for support.

## Appendix A. Supplementary information

Supplementary data associated with this article can be found in the online version at http://dx.doi.org/10.1016/j.nanoen.2014.02.014.

## References

[1] P. Simon, Y. Gogotsi, Acc. Chem. Res. 46 (2013) 1094.
[2] Y. Gogotsi, P. Simon, Science 334 (2011) 917.
[3] X. Xiao, L. Yuan, J. Zhong, T. Ding, Y. Liu, Z. Cai, Y. Rong, H. Han, J. Zhou, Z.L. Wang, Adv. Mater. 23 (2011) 5440.
[4] Q. Zhong, J. Zhong, B. Hu, Q. Hu, J. Zhou, Z.L. Wang, Energy Environ. Sci. 6 (2013) 1779.
[5] M.F. El-Kady, R.B. Kaner, Nat. Commun. 4 (2013) 1475.
[6] J.R. Miller, P. Simon, Science 321 (2008) 651.
[7] Z.S. Wu, K. Parvez, X. Feng, K. Mullen, Nat. Commun. 4 (2013) 2487.
[8] T. Brezesinski, J. Wang, S.H. Tolbert, B. Dunn, Nat. Mater. 9 (2010) 146.
[9] V. Augustyn, J. Come, M.A. Lowe, J.W. Kim, P.-L. Taberna, S.H. Tolbert, H.D. Abruña, P. Simon, B. Dunn, Nat. Mater. 12 (2013) 518.
[10] J. Chmiola, C. Largeot, P.-L. Taberna, P. Simon, Y. Gogotsi, Science 328 (2010) 480.
[11] L.Y. Yuan, B. Yao, B. Hu, K.F. Huo, W. Chen, J. Zhou, Energy Environ. Sci. 6 (2013) 470.
[12] (a) Y. Zhu, S. Murali, M.D. Stoller, K.J. Ganesh, W. Cai, P.J. Ferreira, A. Pirkle, R.M. Wallace, K.A. Cychosz, M. Thommes, D. Su, E.A. Stach, R.S. Ruoff, Science 332 (2011) 1537;
(b) X. Li, B. Wei, Nano Energy 1 (2012) 479.
[13] (a) J. Ren, W. Bai, G. Guan, Y. Zhang, H. Peng, Adv. Mater. 25 (2013) 5965;
(b) B. Yao, L. Yuan, X. Xiao, J. Zhang, Y. Qi, J. Zhou, J. Zhou, B. Hu, W. Chen, Nano Energy 2 (2013) 1071.
[14] X. Lu, T. Zhai, X. Zhang, Y. Shen, L. Yuan, B. Hu, L. Gong, J. Chen, Y. Gao, J. Zhou, Y. Tong, Z.L. Wang, Adv. Mater. 24 (2012) 938.
[15] T. Zhai, F. Wang, M.H. Yu, S. Xie, C. Liang, C. Li, F. Xiao, R. Tang, Q. Wu, X.H. Lu, Y. Tong, Nanoscale 5 (2013) 6790.
[16] K. Wang, W. Zou, B. Quan, A. Yu, H. Wu, P. Jiang, Z. Wei, Adv. Energy Mater. 1 (2011) 1068.
[17] Z. Weng, Y. Su, D.-W. Wang, F. Li, J. Du, H.-M. Cheng, Adv. Energy Mater. 1 (2011) 917.
[18] M.F.L. De Volder, S.H. Tawfick, R.H. Baughman, A.J. Hart, Science 339 (2013) 535.
[19] S. Iijima, Nature 354 (1991) 56.
[20] E. Frackowiak, F. Béguin, Carbon 39 (2001) 937.
[21] J. Shen, A. Liu, Y. Tu, G. Foo, C. Yeo, M.B. Chan-Park, R. Jiang, Y. Chen, Energy Environ. Sci. 4 (2011) 4220.
[22] M. Seredych, D. Hulicova-Jurcakova, G.Q. Lu, T.J. Bandosz, Carbon 46 (2008) 1475.
[23] Y.-R. Nian, H. Teng, J. Electrochem. Soc. 149 (2002) A1008.
[24] C.-T. Hsieh, H. Teng, Carbon 40 (2002) 667.
[25] X. Xiao, X. Peng, H. Jin, T. Li, C. Zhang, B. Gao, B. Hu, K. Huo, J. Zhou, Adv. Mater. 25 (2013) 5091.
[26] S.D. Perera, B. Patel, N. Nijem, K. Roodenko, O. Seitz, J.P. Ferraris, Y.J. Chabal, K.J. Balkus, Adv. Energy Mater. 1 (2011) 936.
[27] G. Lota, J. Tyczkowski, R. Kapica, K. Lota, E. Frackowiak, J. Power Sources 195 (2010) 7535.
[28] C.E. Banks, T.J. Davies, G.G. Wildgoose, R.G. Compton, Chem. Commun. 7 (2005) 829-841.
[29] X. Xiao, T. Ding, L. Yuan, Y. Shen, Q. Zhong, X. Zhang, Y. Cao, B. Hu, T. Zhai, L. Gong, J. Chen, Y. Tong, J. Zhou, Z.L. Wang, Adv. Energy Mater. 2 (2012) 1328.
[30] J. Zhang, J. Jiang, H. Li, X.S. Zhao, Energy Environ. Sci. 4 (2011) 4009.
[31] G.R. Li, Z.L. Wang, F.L. Zheng, Y.N. Ou, Y.X. Tong, J. Mater. Chem. 21 (2011) 4217.
[32] M.F. El-Kady, V. Strong, S. Dubin, R.B. Kaner, Science 335 (2012) 1326.
[33] X. Xiao, T. Li, P. Yang, Y. Gao, H. Jin, W. Ni, W. Zhan, X. Zhang, Y. Cao, J. Zhong, L. Gong, W.C. Yen, W. Mai, J. Chen, K. Huo, Y.L. Chueh, Z.L. Wang, J. Zhou, ACS Nano 6 (2012) 9200.
[34] P. Yang, X. Xiao, Y. Li, Y. Ding, P. Qiang, X. Tan, W. Mai, Z. Lin, W. Wu, T. Li, H. Jin, P. Liu, J. Zhou, C.P. Wong, Z.L. Wang, ACS Nano 7 (2013) 2617.
[35] L. Yuan, X.H. Lu, X. Xiao, T. Zhai, J. Dai, F. Zhang, B. Hu, X. Wang, L. Gong, J. Chen, C. Hu, Y. Tong, J. Zhou, Z.L. Wang, ACS Nano 6 (2012) 656.
[36] Y.J. Kang, H. Chung, C.-H. Han, W. Kim, Nanotechnology 23 (2012) 065401.
[37] M. Kaempgen, C.K. Chan, J. Ma, Y. Cui, G. Gruner, Nano Lett. 9 (2009) 1872.
[38] L. Yuan, X. Xiao, T. Ding, J. Zhong, X. Zhang, Y. Shen, B. Hu, Y. Huang, J. Zhou, Z.L. Wang, Angew. Chem. Int. Ed. 51 (2012) 4934.
[39] X. Lu, D. Zheng, T. Zhai, Z. Liu, Y. Huang, S. Xie, Y. Tong, Energy Environ. Sci. 4 (2011) 2915.
[40] T. Chen, L. Qiu, Z. Yang, Z. Cai, J. Ren, H. Li, H. Lin, X. Sun, H. Peng, Angew. Chem. Int. Ed. 51 (2012) 11977.

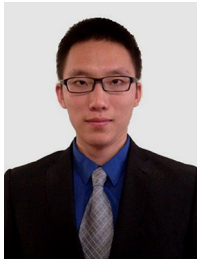

**Xu Xiao** received his B.S. degree from the School of Physics, Huazhong University of Science and Technology (HUST), PR China in June 2011. He is a Ph.D. candidate at Wuhan National Laboratory for Optoelectronics (WNLO) and School of Optical and Electronic Information at HUST. His research interests include flexible electronics and flexible solid-state supercapacitors for self-powered systems.

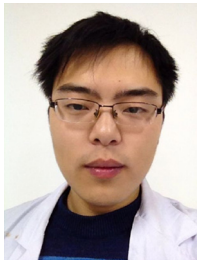

**Tianqi Li** received his Bachelor's degree in Chemistry from Huazhong University of Science and technology. He is a Ph.D. candidate at Wuhan National Laboratory for Optoelectronics (WNLO). His research interest includes supercapacitors for self-powered system.

**Zehua Peng** received his B.S. degree in Optical Information of Science and Technology from Huazhong University of Science and Technology (HUST), PR China in 2013. From March 2013 until now, he is a Research Assistant at Wuhan National Laboratory for Optoelectronics (WNLO) at Huazhong University of Science and Technology (HUST). His research interest includes flexible solid-state supercapacitors for self-powered systems.

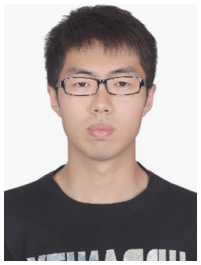

**Huanyu Jin** received his Bachelor's degree from the Huazhong University of Science and Technology in 2013. Now he is an M. Phil. student at The Hong Kong Polytechnic University. His research interests include supercapacitor, various nanocomposite materials, and their applications.

**Qize Zhong** received his B.S.degree in Optoelectronic Information from Huazhong University of Science and Technology (HUST), PR China in June 2011. He is a Ph.D. candidate at Wuhan National Laboratory for Optoelectronics (WNLO) and School of Optical and Electronic Information at HUST. His research interests include flexible electronics.

**Qiyi Hu** received her B.S. degree in Optical information from Hubei College of Engineering, PR China in June, 2011. She is a Master's degree candidate at Wuhan National Laboratory for Optoelectronics (WNLO). Her research interest includes energy harvesting for self-powered system.

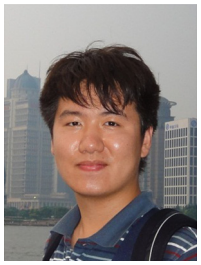

**Bin Yao** received his B.S. degree in Materials Chemistry from Wuhan University of Technology (WUT), China in 2009. He is a master candidate in Material Science at WUT. From 2012 until now, he is a visiting student at Wuhan National Laboratory for Optoelectronics (WNLO) and School of Optical and Electronic Information at Huazhong University of Science and Technology (HUST). His research interest includes flexible solid-state energy storage devices based on conducting polymers and metal oxides.

**Qiuping Luo** received her Ph.D. degree from Sun-Yat Sen University in June 2012, PR China. Since July 2012, she has been working at Wuhan National Laboratory for Optoelectronics (WNLO) as a postdoctoral fellow. Her research interests are focused on fabrication of semiconductor nanomaterials and their applications in photochemistry and supercapacitors.

**Chuanfang Zhang** received his M.Sc. from East China University of Science and Technology, Shanghai, China in 2011 and is now a Ph.D. candidate at Drexel University, Philadelphia, USA under the supervision of Prof. Yury Gogotsi. His research interests mainly lie on the transition metal oxide/carbon composites for supercapacitor and Li-ion battery. Meanwhile, as a passionate researcher, he also developed various advanced electrode fabrication techniques and optimized fundamental testing methods for supercapacitor. Currently he is working on two-dimensional carbides for promising energy storage application.

**Li Gong** received his B.S. and M.S. degree from Key Lab of Display Materials and Technology of Guangdong Province, Sun Yat-Sen University, PR China. He is a lab technician at Instrumental Analysis & Research Center in Sun Yat-Sen University. He is working on photoelectron spectrometer.

**Jian Chen** received his Ph.D. degree in Physics from Sun Yat-sen University in 2001. He is currently a Professor at Instrumentation Analysis and Research Center, Sun Yat-sen University, Guangzhou, China. His research interests are focused on the structure characteristic and compositions of the material surface and interface. He has co-authored more than 100 journal papers. He has received China National Nature & Science Award 2001and other awards for his research.

**Yury Gogotsi** is a Distinguished University Professor and Trustee Chair of Materials Science and Engineering at Drexel University. He also serves as Director of the A.J. Drexel Nanotechnology Institute. His Ph.D. is in Physical Chemistry from Kiev Polytechnic and D.Sc. in Materials Engineering from Ukrainian Academy of Sciences. He works on nanostructured carbons and other nanomaterials for energy related and other applications. He has co-authored more than 370 journal papers and obtained more than 40 patents. He has received numerous national and international awards for his research and was elected a Fellow of AAAS, MRS, ECS and ACerS and a member of the World Academy of Ceramics.

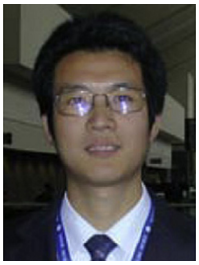

**Jun Zhou** received his B.S. degree in Material Physics (2001) and his Ph.D. in Material Physics and Chemistry (2007) from Sun Yat-Sen University, China. During 2005–2006, he was a visiting student at Georgia Institute of Technology. After obtaining his Ph.D., he worked in Georgia Institute of Technology as a Research Scientist. He joined Wuhan National Laboratory for Optoelectronics (WNLO), Huazhong University of Science and Technology (HUST) as a Professor from the end of 2009. His main research interest includes flexible energy harvesting and storage devices.